Journal of ELECTRONIC MATERIALS, Vol. 43, No. 1, 2014
DOI: 10.1007/s11664-013-2840-4

Evaluation of Electromigration Behaviors of Pb-Free Microbumps in Three-Dimensional Integrated Circuit Packaging

HAO HSU,[1] TZU-YANG LIN,[1] and FAN-YI OUYANG[1,2]

1.—Department of Engineering and System Science, National Tsing Hua University, Hsinchu 300, Taiwan, ROC. 2.—e-mail: fyouyang@ess.nthu.edu.tw

This study investigated electromigration (EM) behaviors of Pb-free microbumps in three-dimensional integrated circuit (3D IC) packaging under electrical current stressing from 1×10^4 A/cm^2 to 1×10^5 A/cm^2 at ambient temperature of 150°C. EM-induced fast under bump metallization consumption at the cathode of the microbumps was observed when the current density was higher than 8×10^4 A/cm^2, whereas no EM-induced damage of the microbumps was found after 14,416 h when the current density was below 1.5×10^4 A/cm^2. We propose that the different EM behaviors of the microbumps were mainly due to the effect of back stress. The critical microbump height to trigger EM for different current densities is discussed, and the resistance evolution of samples during current stressing was found to be correlated with the microstructure of the samples. When the resistance was stable through the whole test period, microscopic inspection of the 3D IC samples indicated that the whole microbumps were transformed to intermetallic compounds without significant EM-induced damage. However, the resistance evolution of some misaligned microbumps exhibited a feature of an early spike along with a huge resistance fluctuation during current stressing. When the resistance abruptly increased after lengthy stressing, EM-induced void formation was observed at the cathode side of the Al trace.

Key words: Electromigration, Pb-free, 3D IC, voids on Al trace, intermetallic compound

INTRODUCTION

To meet demands for higher packaging density, better performance, and smaller feature size in consumer electronic products, packaging technology is currently transitioning from flip-chip technology toward three-dimensional integrated circuit (3D IC) packaging. In 3D IC devices, different Si chips are stacked and connected using microbumps and through-silicon vias (TSVs). When compared with the size of solder joints in flip-chip technology (100 μm), smaller dimensions of the microbumps, approximately 10 μm, are adopted in 3D ICs to provide much shorter electrical paths. However, in such small size microbumps, the current densities applied in the microbumps will dramatically increase. Furthermore, when different Si chips are stacked together, the peak temperature of 3D IC devices will also significantly increase due to intense Joule heating. Thus, addressing reliability problems related to microbumps is critical for this newly developed technology.

In flip-chip technology, electromigration (EM) in solder joints has been regarded as one of the serious reliability problems. Several studies[1–4] have reported that EM-induced failure occurs in the solder joints when the current density in the joints approaches 10^4 A/cm^2. The dominant EM failure mechanism in solder joints is pancake-type void formation and propagation at the solder/intermetallic compound (IMC) interface.[5,6] Owing to the unique bump (solder)-to-line (Al) configuration of flip-chip joints, current crowding generated in the

(Received April 29, 2013; accepted October 4, 2013; published online October 31, 2013)

transition region from the bump to the conducting Al traces[7,8] results in 10 to 20 times higher current density in the current-crowding region as compared with the average current density of the bumps. Thus, voids are prone to initiate in the current-crowding region when electrons travel from the interconnects toward the solder joints (downward electron flow). Once voids are formed, the electrons must pass the front edge of the voids to enter the solder joints, and the current-crowding region is shifted to the new entry of the electrons. Consequently, the voids gradually propagate through the whole cathode contact of the solder joint during current stressing, finally leading to open-circuit failure in electronic devices. In addition, current crowding may cause rapid dissolution of under bump metallurgy (UBM) into Sn-based solders to form IMCs. The flux divergence between the diffusion rate of the UBM and the Sn may also lead to Kirkendall void formation.[9]

The International Technology Roadmap for Semiconductors (ITRS) has predicted that the power of electronic devices will increase and the maximum temperature of devices will reach 150°C under harsh operating conditions. Thus, this study aims to evaluate the EM behaviors of Pb-free microbumps in 3D IC packaging under electrical current stressing ranging from 1×10^4 A/cm^2 to 1×10^5 A/cm^2 at ambient temperature of 150°C. The resistance evolution of the samples during current stressing was correlated with microstructural observations of the microbumps. Possible failure mechanisms of the microbumps induced by EM are also discussed.

EXPERIMENTAL PROCEDURES

Materials

This study used 3D IC samples provided by the Industrial Technology Research Institute of Taiwan (ITRT). The samples consisted of a top chip and a bottom chip, with microbumps in between. The dimensions of the top chip and bottom chip were 5 mm × 5 mm and 15 mm × 15 mm, respectively. The thickness of both chips was 0.75 mm. To fabricate 3D IC samples (Fig. 1a), Al was first deposited as bump pads with diameter of 20 μm on both chips. UBM thin films of Cu (ca. 3 μm)/Ni (ca. 5 μm) were then deposited on the Al bond pads using electroplating. The contact opening between the Al bond pad and the Cu UBM had a diameter of 12 μm. Next, Pb-free Sn-2.5Ag solder, with a thickness of 5 μm, was electroplated on the Ni UBM.

Prior to the assembly process, a plasma treatment was implemented to remove oxidation and contamination on the sample surface and to improve the wettability. To assemble the top and bottom chips, Suss FC-150 and Toray FC3000WS bonders were used for high-accuracy alignment, followed by a thermocompressive bonding process with peak temperature of 280°C for 40 s. Subsequently, a capillary underfill was dispensed in the gap between the two chips, and the samples were then cured at 150°C for 30 min. After the thermocompressive bonding, the structure of the microbumps, Cu/Ni/Sn-2.5Ag/Ni/Cu, is shown in Fig. 1b. Ni_3Sn_4 IMC (ca. 1 μm) was formed at the interface between the Ni UBM layer and the Sn-2.5Ag solder. The remaining height of the Sn-2.5Ag microbumps between the top and bottom IMCs was estimated to be about 6 μm after the process of thermal compression. Al traces, with 10 μm width and 0.8 μm thickness, were employed to provide a connection between the microbumps.

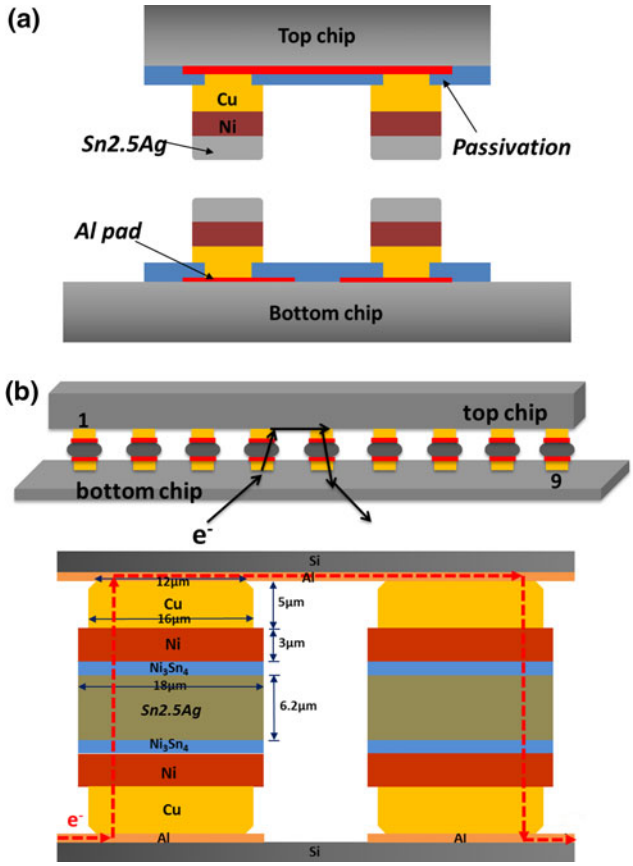

Fig. 1. Schematic representation of (a) 3D IC samples and (b) test structure of 3D IC samples.

Experimental Setup and Characterization

To conduct EM tests, the samples were connected to a power source in constant direct-current (DC) mode and placed in a furnace at ambient temperature of 150°C. The average current density in the microbumps ranged from 1×10^4 A/cm^2 to 1×10^5 A/cm^2, calculated as the applied DC current divided by the area of the passivation opening. As shown in Fig. 1b, the test layout of the samples included an array of nine Pb-free microbumps located on the periphery of the chip. Only one pair of microbumps (no. 4 and no. 5) was current stressed, while the other seven microbumps were

unstressed. Arrows depict the direction of electron flow. The electrons entered the microbump (no. 4) in the lower left-hand corner from the Al pad on the substrate side and exited the microbump from its upper right-hand corner into the Al trace on the chip side. The electrons then flowed along the Al trace, and entered the other stressed microbump (no. 5) from its upper left-hand corner, finally exiting through its lower right-hand corner to the Al trace on the substrate side. During the EM tests, the voltage across the two current-stressed microbumps was recorded *in situ* using a multimeter connected to a computer for data acquisition. By dividing the recorded voltage by the constant current, the resistance was obtained as a function of time. To minimize noise from resistance variation of the connecting wires, four-point probe measurement was employed for the test configuration of the samples. After the EM tests, the samples were slowly cooled down to room temperature in the furnace to minimize the thermal stress induced in the samples.

To understand the distribution of current density in the microbumps, COMSOL Multiphysics engineering simulation software was employed. The settings of the simulation followed the "heat power transistor" model, a built-in example in the COMSOL program. Table I lists the material parameters of the constituent components of the 3D IC samples. The 3D IC module was built using SolidWorks, then imported into the COMSOL program. The study type was chosen to be "stationary," indicating that the results acquired in the simulation were in a stationary state. The mesh for the simulation contained 701,896 elements, with maximum and minimum element sizes of 5.87×10^{-5} m and 5.87×10^{-7} m, respectively.

To observe the microstructure of the microbumps after EM testing, the samples were first ground close to the center of the microbumps using SiC water sandpapers sequentially from no. 180 to no. 4000. Then, the surface of the samples was polished using Al_2O_3 slurries sequentially with particle size of 0.3 μm and 0.05 μm. Finally, the samples were cleaned in deionized water for 1 min. The microstructural changes of the cross-sectioned microbumps were observed using scanning electron microscopy (SEM). The compositional changes and the different phases inside the microbumps were identified by energy-dispersive x-ray (EDX) analysis and electron probe microanalysis (EPMA).

RESULTS AND DISCUSSION

Relationship Between the Resistance Curve and Microstructural Evolution

The results for the initial resistance, percentage resistance increase, and stressing time of six samples are summarized in Table II. The initial resistance of all samples ranged from 23.16 Ω to 24.59 Ω, showing no significant variation of the initial resistance among the as-received samples. The corresponding resistance versus time (RVT) curves for the samples under current stressing at 150°C are shown in Fig. 2; three types of RVT curves were observed. When the RVT curve was extremely stable through the whole stressing period, it was defined as a type I curve. For a type II curve, an early spike of resistance was observed, accompanying resistance fluctuation after lengthy current stressing. When the resistance was stable and then abruptly increased in the final stage of current stressing, we defined it as a type III curve.

A type I curve was observed for sample A, indicating that the corresponding RVT curve was quite flat through the whole current stressing time of 14,416 h, along with a slight increase of resistance by 0.3%. Figure 3a and b show the microstructure of the current-stressed microbumps (1×10^4 A/cm^2) and the unstressed neighboring microbumps at 150°C after 14,416 h (approximately 20 months), respectively. As shown in Fig. 3a, the traditional failure mode in flip-chip technology, i.e., pancake-type voids at the solder/IMC interface, was not detected in either current-stressed microbump. Meanwhile, a symmetrical microstructure was observed on the current-stressed microbumps. Due to Joule heating induced by the electrical current, the entire microbumps experienced phase transformation into Ni_3Sn_4 IMC after a long period of current stressing. We also found that $(Ni,Cu)_3Sn$ IMC was formed at the upper left-hand corner of the microbumps regardless of the direction of electron flow. In addition, both current-stressed and neighboring unstressed microbumps exhibited similar microstructural evolution, as evidenced by the SEM image in Fig. 3b. Thus, these results suggest that no EM-induced damage was observed for either current-stressed microbump, in reasonable agreement with the RVT curve results. In addition, several small voids were also found inside the IMCs. These voids were considered to be induced during IMC formation; when Ni_3Sn_4 and $(Ni,Cu)_3Sn$ IMCs are

Table I. Material parameters of the constituent components of the 3D IC samples

Material	Cu	Al	Ni	Sn-2.5Ag	Ni_3Sn_4
Electrical conductivity (S/m)	3.81×10^7	3.55×10^7	1.38×10^7	8.12×10^6	3.51×10^6
Specific heat at constant pressure (J/kg K)	384	904	445	220	272
Density (kg/m^3)	8960	2700	8900	7400	8650
Thermal conductivity (W/m K)	401	237	90.7	78	196

Table II. Experimental results of 3D IC samples tested in this study

Sample	A	B	C	D	E	F
Temperature (°C)	150	150	150	150	150	150
Current density (A/cm^2)	1×10^4	1.5×10^4	3×10^4	6×10^4	8×10^4	1×10^5
Stressed period (h)	14,416	14,420	1249	7830	4950	2903
Initial resistance (Ω)	23.16	23.93	23.74	23.75	23.85	24.59
Highest resistance (Ω)	23.22	24.08	59.15	29.97	26.59	26.56
Max. resistance increase (%)	0.3	0.6	149.2	26.2	11.5	8.0
Type of RVT curve during stressing	Type I	Type I	Type II	Type II	Type III	Type III

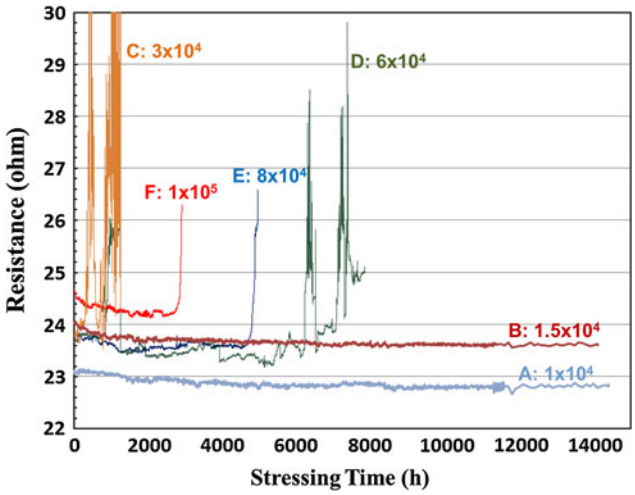

Fig. 2. Resistance as a function of stressing time under different current densities at ambient temperature of 150°C.

formed, the volume shrinks by approximately −11.4% and −7.5%, respectively. Additionally, some Ag_3Sn IMC was found in the middle of the Ni_3Sn_4 phase. Because of the negligible solubility of Ag in Ni_3Sn_4, Ag atoms would be excluded from the Ni_3Sn_4 phase during the current-stressing process[10,11] and form Ag_3Sn IMC. As the remaining solder was gradually consumed and transformed into Ni_3Sn_4, the Ag_3Sn ended up located at the center of the microbumps. Sample B exhibited a similar resistance change and microstructural evolution after undergoing current stressing of 1.5×10^4 A/cm^2 for 14,420 h: a flat resistance curve was observed during the entire EM test period, and both current-stressed microbumps were completely transformed into IMCs accompanied by several small voids inside (not shown here).

For both samples C and D, the RVT curves in Fig. 2 are quite flat at the beginning, but an early spike of resistance occurs, then the curve exhibits a huge fluctuation after prolonged stressing (type II). To understand the reason for the early spike in the RVT curves, Fig. 4a and b show cross-sectional SEM images of microbumps under current stressing of 3×10^4 A/cm^2 and 6×10^4 A/cm^2 at 150°C, respectively. Dissimilar to the shape of the microbumps in sample A, misaligned microbumps were observed for both samples C and D. Due to Joule heating, the region connecting the upper and lower UBMs was totally transformed to IMCs after a long period of current stressing, and several voids appeared in the center of the IMC region. Additionally, due to the misalignment of the microbumps, Sn was found to have reacted extensively with the sidewall of the UBM, and thus $(Ni,Cu)_3Sn$ IMC was formed. As electrons would travel the shortest distance inside the microbumps, no electrons flowed through the upper left-hand region of the microbumps for sample C, and thus unreacted Sn solder remained. The early spike of resistance observed for samples C and D can be accredited to the misaligned microbumps formed during the thermocompressive process, which may lead to intrinsic defects in the joints. It is believed that these preexisting defects inside the microbumps can speed up EM-induced failure.[12] Notably, the initial resistance of samples C and D was only slightly different from that of other, well-aligned samples, suggesting that misalignment of microbumps cannot be recognized by measuring their initial resistance. However, once the misaligned samples were subjected to current stressing, the feature of an early spike as well as a huge resistance fluctuation during current stressing can provide an early indication of the poor quality of the samples.

Both samples E and F exhibited a type III curve; the resistance of the samples was flat for a prolonged time and then abruptly increased in the last few hours, as shown in Fig. 2. The resistance increased by 11.4% of its original value in the last 250 h for sample E, and by 8.0% of its original value in the last 50 h for sample F. Figure 5 displays the microstructure of the microbumps after current stressing at 150°C for sample E (8×10^4 A/cm^2), showing that the Sn-based solder inside the whole microbump was totally transformed to Ni_3Sn_4 IMC, and the Ni UBM layer at the cathode was significantly consumed for the microbumps with upward electron flow. These findings imply the occurrence of EM inside the microbumps of sample E. Asymmetrical consumption of Ni and Cu UBMs was also found in the current-crowding region, where electrons traveled from the Al trace into the Cu UBM, thus resulting in $(Ni,Cu)_3Sn$ formation. Additionally, volume shrinkage was observed on the sidewall

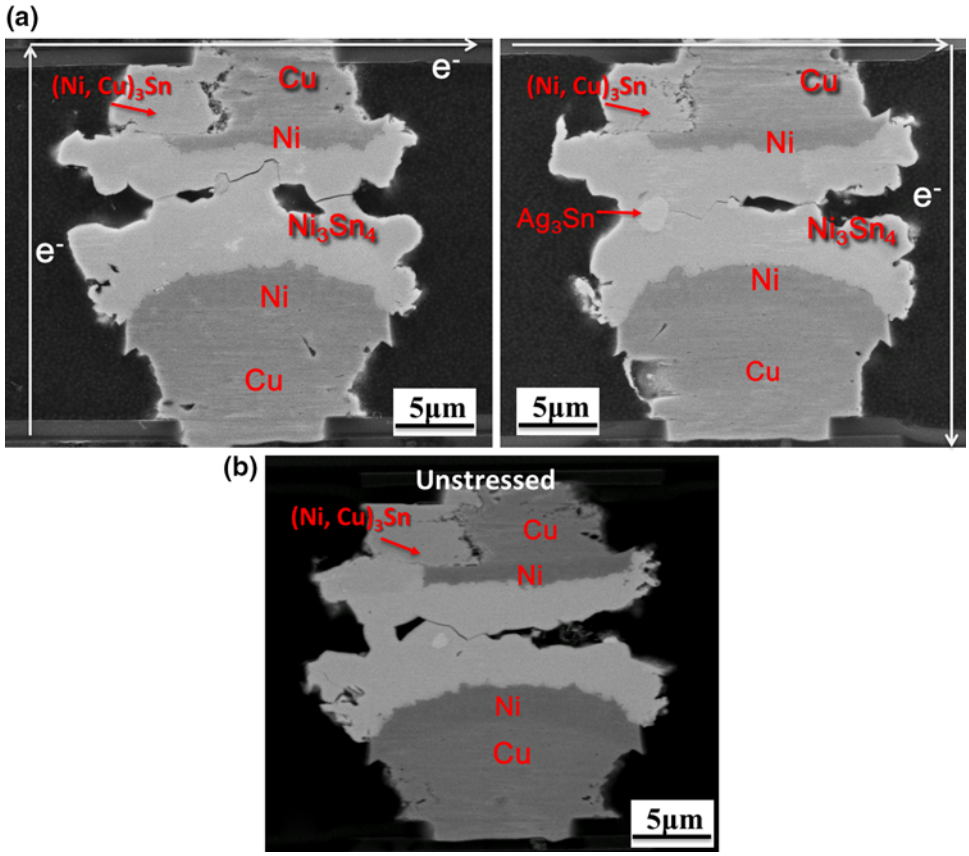

Fig. 3. Cross-sectional SEM images of (a) microbumps after current stressing at 1×10^4 A/cm^2 and (b) unstressed neighboring microbump after 14,416 h at 150°C.

of the microbumps, which was possibly caused by the formation of IMCs. Another large crack appeared at the upper right-hand corner of the microbump with downward electron flow; however, this crack did not propagate through the whole microbump opening. Furthermore, at the lower right-hand corner of the stressed microbump in Fig. 5, a pronounced void was surprisingly observed at the cathode side of the Al trace, as highlighted in the dashed-line region. Figure 6 shows an enlarged image of the voids at the Al trace and an EPMA concentration profile of Al across the Al trace after EM testing. Points were taken at 1 μm intervals, as indicated in Fig. 6. The EPMA results show that only approximately 1 mass% Al was detected in the region of voids from point 8 toward point 14, consistent with the cross-sectional images shown in Fig. 5.

A similar phenomenon was observed for the current-stressed microbumps of sample F (1×10^5 A/cm^2). The results (Fig. 7) show that the whole of both current-stressed microbumps was transformed into IMCs. In addition, the Cu and Ni UBMs were markedly consumed at the cathode of the microbumps with downward electron flow, suggesting the occurrence of EM in the microbumps of sample F. Again, void formation was clearly seen in the cathode of the Al trace, as indicated by the dashed rectangular box in Fig. 7a. To provide a clearer view of the microstructure after EM testing, Fig. 7b shows an enlarged image of the void formation in the Al trace. The voids are 2 μm away from the current-crowding region at the upper right-hand corner of the contact where the electrons entered the microbump from the Al traces.

Figure 8a and b show the simulated current distribution and temperature distribution in microbumps undergoing current stressing at 1×10^5 A/cm^2 (sample F) at 150°C, respectively. As shown in Fig. 8a, the results indicate that the current density was evenly distributed among the microbumps. The maximum current density, 1.74×10^6 A/cm^2, was generated at the corner of the entrance between the Al trace and the Cu UBM. The Al trace between the two current-stressed microbumps also exhibited an average current density of 1.41×10^6 A/cm^2. In addition, one can see that Joule heating induced by current stressing increased the temperature of the Al trace and the microbumps. The highest temperature of the Al trace was around 465 K (202°C), and the temperature of the current-stressed microbumps ranged from 458 K (185°C) to 461 K (188°C).

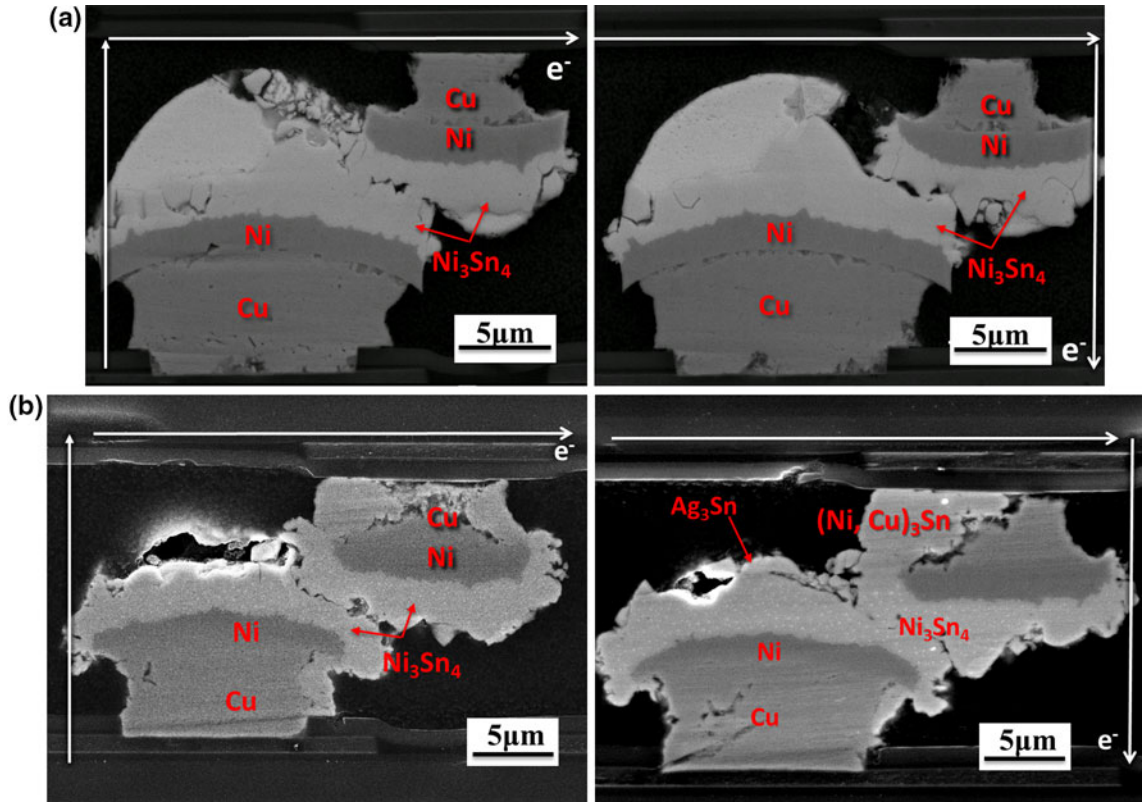

Fig. 4. Cross-sectional SEM images of microbumps after current stressing at (a) 3×10^4 A/cm^2 for 1249 h and (b) 6×10^4 A/cm^2 for 7830 h at 150°C.

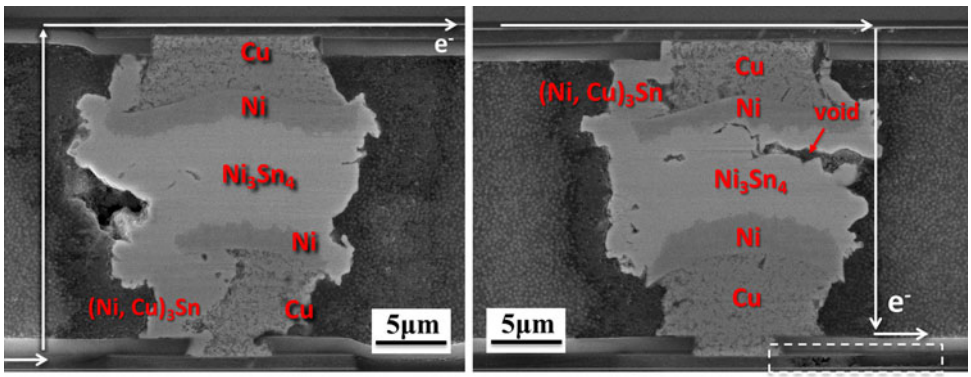

Fig. 5. Cross-sectional SEM images of microbumps after current stressing at 8×10^4 A/cm^2 at 150°C for 4950 h.

Electromigration in Microbumps

Comparing the microstructural evolution of microbumps subjected to different current densities, we find symmetrical microstructural evolution inside the microbumps for samples A, B, C, and D, suggesting no EM-induced damage in the microbumps stressed at lower current densities. However, EM occurred in the current-stressed microbumps of samples E and F, as evidenced by the fast UBM consumption at the cathode of the microbumps. An explanation for the different microstructural evolution of the microbumps for samples A, B, C, and D versus samples E and F can be given by considering the effect of back stress in the microbumps. Similar to what has been widely observed for EM in Al strips and solders,[3,14,15] when the electrical current drives Sn atoms to move from the cathode to the anode, a built-in stress gradient is developed across the solder joint, and thus a reverse flux moving from the anode to the cathode is induced. As a result, the total atomic flux caused by current stressing and back stress can be expressed as

$$J_{\mathrm{em}} = -C\frac{D}{kT}\frac{\mathrm{d}\sigma\Omega}{\mathrm{d}x} + C\frac{D}{kT}Z^{*}eE, \qquad (1)$$

where J_{em} is the atomic flux (atoms/cm^2 s), C is the concentration of atoms per unit volume, D/kT is the atomic mobility, σ is the stress, Ω is the atomic volume, Z^* is the effective charge number for EM, and E is the electric field ($E = \rho j$, where ρ is the resistivity and j is the current density). When the contribution from the flux due to the electrical current and the back stress become equal, Eq. 1 can be rearranged as follows:

$$\Delta x \cdot j_c = \frac{\Delta\sigma\Omega}{Z^* e\rho}. \quad (2)$$

In the above equation, $\Delta x{\cdot}j_c$ can be regarded as a critical product for the solder, indicating that there will be no net effect of EM of Sn when the experimental value of $\Delta x{\cdot}j$ is below this critical product value. Because Joule heating would increase the temperature of the microbumps and the stress gradient (back stress) is temperature dependent, we should consider the case with Joule heating; that is, the actual temperature of the microbumps would be 150°C plus the Joule heating. Because the samples stressed by lower current densities would produce smaller Joule heating and have much lower temperatures, sample F with the highest Joule heating generated from the current density of 1×10^5 A/cm^2, that is, 188°C (150°C + 33°C) based on the simulation results in Fig. 8b, was used as a harsh scenario for the calculation. If we take Y (Young's modulus) = 26 GPa and 19 GPa for Sn-Ag solder at 150°C and 188°C,[16] respectively, and assume σ to be the elastic limit, $\Delta\sigma$ would be 5.2×10^7 Pa at 150°C and 3.8×10^7 Pa at 188°C. Then, taking $\Omega = 16.3$ cm^3/mole, $\rho = 13.25$ $\mu\Omega$ cm, and $Z^* = 17$[9] for Sn, the critical product can be estimated. Based on Eq. 2, the critical bump height to trigger EM can be calculated for a given current density applied in the microbumps.

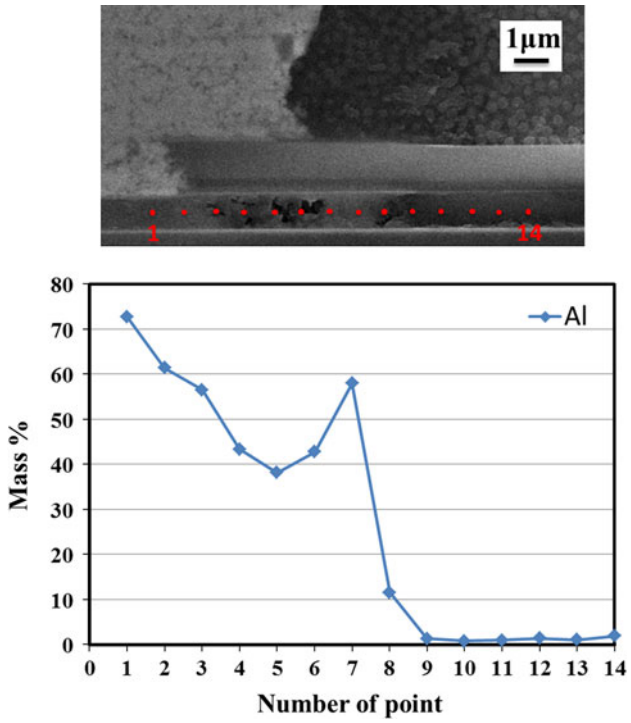

Fig. 6. EPMA concentration profile of Al across the Al trace after EM testing.

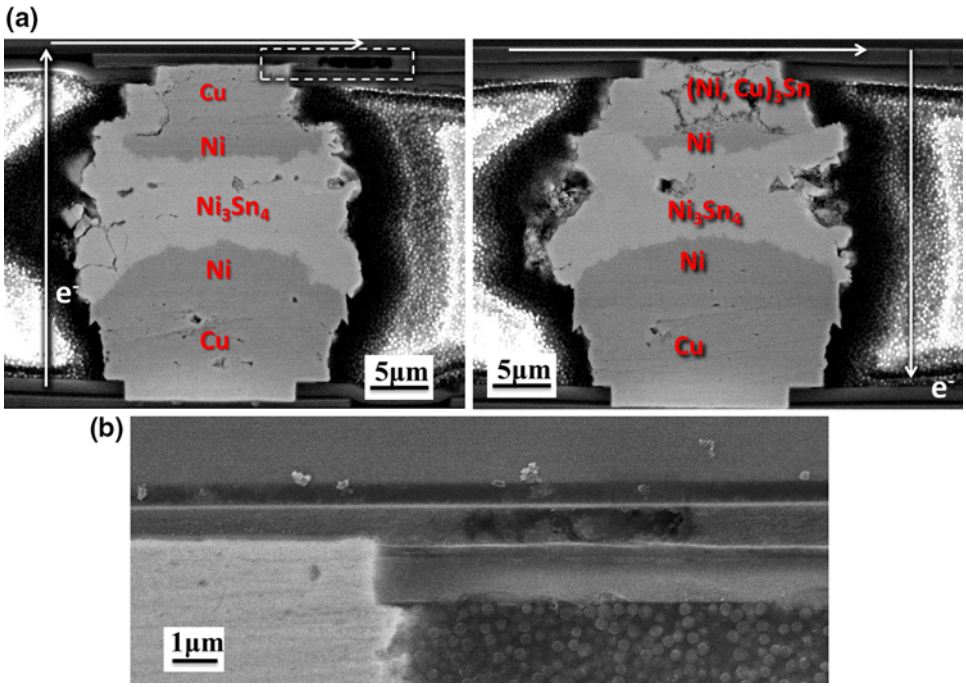

Fig. 7. (a) Cross-sectional SEM images of microbumps after current stressing at 1×10^5 A/cm^2 at 150°C for 2903 h, and (b) enlarged image of void formation at the cathode of the Al trace.

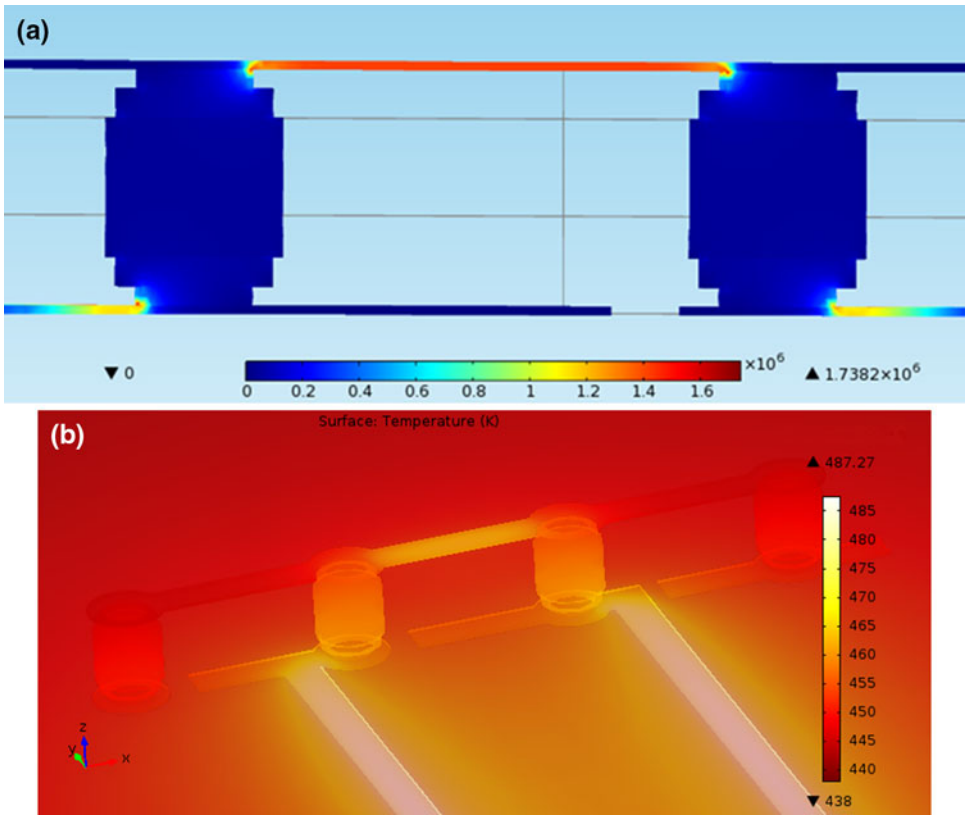

Fig. 8. Simulated (a) current distribution and (b) temperature distribution of 3D IC microbumps under current stressing at 1×10^5 A/cm^2 at 150°C.

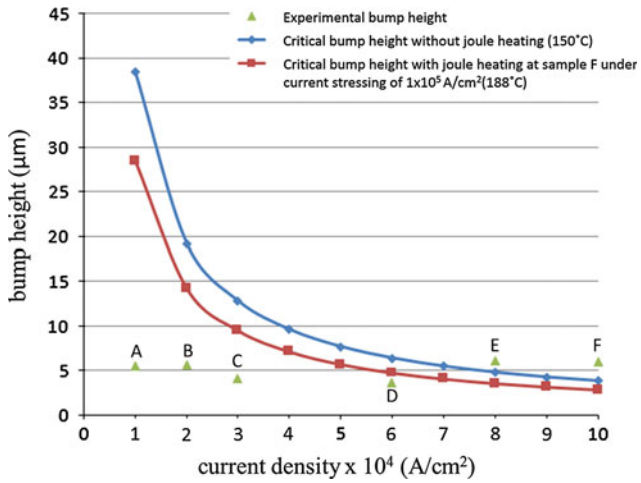

Fig. 9. Critical bump height to trigger EM for different current densities at 150°C.

Figure 9 shows the critical bump height to trigger EM of Sn for different current densities when the temperature is 150°C and 188°C. For the 3D IC samples in this study, the microbump height is approximately 4 μm to 7 μm. Thus, for samples A, B, C, and D, the bump heights did not reach the critical value; this fact suggests that the driving force for EM was counteracted by the effect of back stress, thereby leading to a significant improvement of EM resistance. However, the difference in the chemical potential between Sn and Ni would still drive IMC formation. Because the Joule heating induced by the electrical current would increase the temperature of the samples and in turn accelerate the growth of IMCs, the whole microbumps were gradually transformed into IMCs during the EM test period. Furthermore, IMCs have been reported to possess better EM resistance,[17] further explaining why no EM-induced damage was observed in 3D IC samples under current stressing of 1×10^4 A/cm^2 to 6×10^4 A/cm^2.

On the other hand, the bump heights of samples D and E exceeded the calculated critical bump height, suggesting that EM overwhelmed the effect of back stress. In other words, this indicates that Sn atoms were transported from the cathode to the anode in response to the driving force for EM. The influence of the electron flow is evidenced by the polarity effect observed in samples E and F (Fig. 5). However, due to the serious Joule heating induced by the high current density, the whole microbumps were finally transformed into IMCs, which further provided better EM resistance. It is worth noting that the 3D IC samples were capable of withstanding a higher current density (up to 10^5 A/cm^2) and exhibited better EM resistance compared with flip-chip technology, as shown by the

fact that flip-chip solder bumps typically fail no later than 1500 h under current stressing at 10^4 A/cm^2.[9] Similar observations of better EM performance of 3D IC technology are also indicated in the literature.[4,13] In addition to better EM resistance due to IMC formation, another reason for the relatively longer lifetime could be attributed to the introduction of thicker Cu and Ni UBMs in the 3D IC samples. As evidenced by the simulation results in Fig. 8a, the current density (10^5 A/cm^2) was found to be uniformly distributed throughout the whole microbumps. Meanwhile, current crowding occurred at the corner of the Cu UBM connected to the Al trace in the 3D IC samples, instead of at the connection between the bump and the trace, which is the traditional current-crowding region in flip-chip samples.[3,4] Due to this different current-crowding region in the 3D IC samples, the microbumps in the 3D IC samples thus exhibit better resistance against EM.

Thermomigration in Microbumps

In addition to EM, the effect of thermomigration (TM) should also be considered in the microbumps, as some literature[18,19] has reported that TM may accompany EM to induce failure in flip-chip technology. Based on the simulated temperature distribution for the microbumps of sample F (1×10^5 A/cm^2) in Fig. 8b, a temperature gradient was generated across the microbump. The temperature distribution inside the microbump ranged from 185°C to 188°C, showing a difference of 3°C across the microbump. To roughly estimate the critical temperature gradient to trigger TM, we can compare the driving forces for TM versus EM. Let us recall that the samples subjected to current density of 8×10^4 A/cm^2 and 8×10^8 A/m^2 exhibited EM in the microbumps. The driving force for EM is $F = Z^*eE = Z^*e\rho j$. Taking $\rho = 13.25\ \mu\Omega$ cm and $Z^* = 17$[9] with $e = 1.602 \times 10^{-19}$ C, one has $F = 17 \times 1.6 \times 10^{-19}$ (C) $\times$ 13.25×10^{-8} (Ω m) $\times$ 8×10^8 A/m^2 $= 2.89 \times 10^{-16}$ C V/m $= 2.89 \times 10^{-16}$ N. Thus, for an atom to jump a distance of 3×10^{-10} m, the work done by the EM force will be $\Delta w = 8.67 \times 10^{-26}$ N m $= 8.67 \times 10^{-26}$ J.

To enable an atom to jump across a distance of 3×10^{-10} m under the influence of a temperature gradient, the change of thermal energy should be the same as the work done by the EM force (8.67×10^{-26} J); the change of thermal energy would be $3k\Delta T = 3 \times 1.38 \times 10^{-23}$ (J/K) $\times\ \Delta T = 8.67 \times 10^{-22}$ J, where ΔT is the temperature difference. Thus, the temperature difference across an atomic spacing of 3×10^{-10} m would be 2.09×10^{-3} K, and the corresponding temperature gradient would be $2.09 \times 10^{-3}/3 \times 10^{-10}$ m $= 6.9 \times 10^4$ K/cm. In other words, to induce TM in a microbump, a temperature gradient of 6.9×10^4 K/cm would be required. However, according to the simulated temperature distribution for the microbumps of sample F in Fig. 8b, the highest temperature difference of 3 K across the microbump height of 6 μm would produce a temperature gradient of 5×10^3 K/cm, which is insufficient to trigger TM in the microbumps. Note that the temperature difference of 3 K was generated based on the harshest stressing condition in this study. In other words, the temperature difference would be much smaller for the samples stressed under lower current densities. Therefore, the effect of the temperature gradient on the microstructural evolution of the microbumps was insignificant in this study.

Void Formation at the Cathode of the Al Trace

According to the plot of resistance versus time in Fig. 2, the resistance increased abruptly in the final stage of current stressing for samples E and F. Thus, the question is whether this abrupt resistance increase was caused by the microstructural evolution in the stressed microbumps. For samples E and F, because the Joule heating generated by the high current densities (8×10^4 A/cm^2 to 1×10^5 A/cm^2) was quite significant, the Joule heating would accelerate the reaction rate of IMCs. Thus, for the lower microbump height ($\sim$6 μm), the microbumps were quickly transformed into IMC, accompanied by asymmetrical UBM consumption under the influence of EM. However, due to the better EM resistance of the IMCs, it became more difficult for EM to induce damage inside the microbumps as the stressing time increased. Moreover, the formation of IMCs and small voids inside the IMCs cannot explain the abrupt increase of resistance observed in the RVT plot. This proposition can be supported by the results for sample A, which exhibited similar phase transformation along with void formation during EM testing, whereas the resistance remained flat for 14,416 h. Furthermore, it is believed that the contribution of void formation would increase the resistance by only 0.02 mΩ,[17] and the corresponding resistance only increased by 0.02% of its original value when the whole microbumps were transformed into Ni_3Sn_4. Thus, the contribution of the microstructural evolution of the microbumps to the resistance change is negligible.

Besides the microstructural evolution of the microbumps, EM-induced damage was also observed in the Al trace under high current stressing for samples E and F. From the SEM images in Fig. 7, one can see that the damage to the Al trace was severe. Here, we propose that the voids at the cathode of the Al trace are responsible for the abrupt resistance increase observed for samples E and F. Similar to the traditional EM failure mode in the two-level Al/W/Al interconnect structure,[3,14,20] void formation occurs at the cathode of the Al interconnect above microbumps if we replace the microbumps by a pair of W vias. According to the simulation results shown in Fig. 8, the current density in the Al trace was about 1.1×10^6 A/cm^2. Under such a high current density, Al atoms pos-

sessed sufficient energy to be transported from the cathode to anode. Meanwhile, the Joule heating induced by the current stressing increased the temperature of the Al trace to 202°C and in turn facilitated the diffusion of Al. Consequently, voids were formed at the cathode of the Al traces.

To provide preliminary verification of the EM-induced damage to the Al trace, we calculated the activation energy for EM in the Al trace using the time-to-failure equation,

$$\mathrm{TTF} = A\frac{1}{j^n}\exp\left(\frac{E_a}{kT}\right), \quad (3)$$

where A is a constant ($\sim$0.8), j is the current density (A/cm^2), n is the current density exponent, E_a is the activation energy, k is Boltzmann's constant, and T is the average working temperature. Taking the failure time as 4950 h and 2903 h for current density in the Al trace of 8.8×10^5 A/cm^2 and 1.1×10^6 A/cm^2 for sample E and F, respectively, we obtain n as 1.78 and E_a as 1.22 eV. The obtained n value is quite similar to the value (n = 1.8) reported for EM in Al interconnects.[21–23] Meanwhile, the value of E_a calculated in this study is also in reasonable agreement with the value (1.2 eV) obtained from Black's experiment,[24,25] where EM testing was conducted on 0.7-μm-thick deposited Al films with SiO_2 coating on the surface. Thus, the above-mentioned results further confirm that voids at the cathode of the Al traces were responsible for the abrupt increase for samples E and F.

Another interesting observation is that the voids did not form near the current-crowding region, i.e., in the corner of the Cu UBM connected to the Al trace. Instead, the voids were formed approximately 2 μm away from the current-crowding region. We speculate that the voids formed away from the current-crowding region were caused by dissolution of Ti and Cu UBMs into the Al trace under the influence of current stressing. This proposition is supported by the EPMA results, which show the existence of Cu and Ti signals in the Al trace. When electrons traveled from the Cu UBM into the Al trace, dissolution of Cu UBM into Al was effectively prevented by the Ti diffusion barrier; however, once this diffusion barrier was completely broken under high current stressing, this barrier no longer existed, so that a high current density could drive Cu atoms into the Al trace. Consequently, due to the flux divergence between Al and Cu atoms, voids were formed approximately 2 μm from the current-crowding region. To estimate the diffusion length of Cu in Al when the samples were current stressed at 1.1×10^6 A/cm^2, we can take the diffusion coefficient (D) of Cu in Al to be $0.654 \times \exp(-E_a/kT)$, where E_a = 136 kJ/mole,[25] and T is 202°C as obtained from the simulation results in Fig. 8. The diffusion coefficient of Cu in Al is then 2.54×10^{-15} cm^2/s. The diffusion distance (x) of Cu in Al is $x = (Dt)^{1/2}$. As t is 2903 h for sample F, x can be calculated as 1.63 μm, which is in reasonable agreement with the observed void location in Fig. 7.

CONCLUSIONS

EM behaviors of Pb-free Sn-2.5Ag microbumps in 3D IC package samples were evaluated at ambient temperature of 150°C under current stressing from 1×10^4 A/cm^2 to 1×10^5 A/cm^2 by measuring the resistance evolution and characterizing their microstructure. The results indicated that the resistance evolution could be correlated with the microstructural observations. For current density below 1.5×10^4 A/cm^2, the resistance was stable throughout 14,420 h of current stressing and no EM-induced damage was observed inside the microbump. Instead, the whole microbumps were transformed into IMCs because of the effect of Joule heating. When the current density was increased above 8×10^4 A/cm^2, the resistance was stable for a long time and then abruptly increased. The abrupt increase of resistance was believed to be due to EM-induced voids at the cathode of the Al trace. Meanwhile, the whole microbumps were transformed into IMCs accompanied by fast UBM consumption at the cathode of microbumps, indicating the occurrence of EM inside the microbumps. We propose that the different microstructural evolution of microbumps for low versus high current stressing resulted from the effect of back stress. The critical bump height to trigger electromigration of Sn was calculated to decrease with increasing current density. Furthermore, the RVT curves of misaligned microbumps were found to exhibit the feature of an early spike along with huge resistance fluctuation during current stressing, thereby providing an early indication of poor sample quality.

ACKNOWLEDGEMENT

We thank the National Science Council of Taiwan, ROC, for financial support under Contract No. 102-2221-E-007-051-MY3.

REFERENCES

1. J.D. Wu, P.J. Zheng, C.W. Lee, S.C. Hung, and J.J. Lee, in 41st Annual International Reliability Physics Symposium (IEEE, 2003), pp. 132–139.
2. R. Rosenberg, D.C. Edelstein, C. Hu, and K.P. Rodbell, *Annu. Rev. Mater. Sci.* 30, 229 (2000).
3. E.T. Ogawa, K.-D. Lee, V.A. Blaschke, and P.S. Ho, *IEEE Trans. Reliab.* 51, 403 (2002).
4. A. Syed, K. Dhandapani, L. Nicholls, R. Moody, C.J. Berry, and R. Darveaux, in 10th International Conference and Exhibition on Device Packaging (IMAPS, 2010), pp. 166–171.
5. L. Zhang, S. Ou, J. Huang, K.N. Tu, S. Gee, and L. Nguyen, *Appl. Phys. Lett.* 88, 012106 (2006).
6. E.C.C. Yeh, W.J. Choi, K.N. Tu, P. Elenius, and H. Balkan, *Appl. Phys. Lett.* 80, 580 (2002).
7. R.R. Tummala and S.M. Kamath, *Fundamentals of Microsystems Packaging* (New York: McGraw-Hill, 2001), pp. 264–293.
8. T.Y. Lee, K.N. Tu, and D.R. Frear, *J. Appl. Phys.* 90, 4502 (2001).

9. K.N. Tu, *Solder Joint Technology: Materials, Properties, and Reliability* (New York: Springer, 2007).
10. C. Schmetterer, H. Flandorfer, K.W. Richter, and H. Ipser, *J. Electron. Mater.* 11, 1415 (2007).
11. C.E. Ho, S.C. Yang, and C.R. Kao, *J. Mater. Sci. Mater. Electron.* 18, 2007 (155).
12. Z. Tang and F.G. Shi, *Microelectron. J.* 32, 605 (2001).
13. F.Y. Ouyang, H. Hsu, Y.P. Su, and T.C. Chang, *J. Appl. Phys.* 110, 123525 (2012).
14. K.N. Tu, *J. Appl. Phys.* 94, 5451 (2003).
15. P.S. Ho and T. Kwok, *Rep. Prog. Phys.* 52, 301 (1989).
16. A. Shirazi, A. Varvani-Farahani, and H. Lu, *Int. J. Fract.* 151, 135 (2008).
17. Y.W. Chang, S.W. Liang, and C. Chen, *Appl. Phys. Lett.* 89, 032103 (2006).
18. A.T. Huang, A.M. Gusak, K.N. Tu, and Y.S. Lai, *Appl. Phys. Lett.* 88, 141911 (2006).
19. F.Y. Ouyang and C.L. Kao, *J. Appl. Phys.* 110, 123525 (2011).
20. J.M. Poate, K.N. Tu, and J.W. Mayer, *Thin Films Interdiffusion and Reactions* (New York: Wiley-Interscience, 1978).
21. A. Syed, K. Dhandapani, R. Moody, L. Nicholls, and M. Kelly, in Electronic Components and Technology Conference (IEEE, 2011), pp. 332–339.
22. T.Y. Lee, K.N. Tu, S.M. Kuo, and D.R. Frear, *J. Appl. Phys.* 89, 3189 (2001).
23. W.J. Choi, E.C.C. Yeh, and K.N. Tu, *J. Appl. Phys.* 94, 5665 (2003).
24. J.R. Black, *IEEE Trans. Electron Devices* 16, 338 (1969).
25. W.F. Gale and T.C. Totemeier, *Smithells Metals Reference Book* (Oxford: Elsevier Butterworth-Heinemann, 2004).